A Low-Cost Wearable Device for Portable Sequential Compression Therapy

Running Title: ***Low-Cost Wearable Sequential Compression Therapy***

Mark Schara[1,†], Mingde Zeng[1,†], Barclay Jumet[1,††,*], Daniel J. Preston[1,††,*]

[1] Department of Mechanical Engineering, Rice University, Houston, TX, USA

[†] These authors contributed equally to this work and share first authorship.
[††] These authors contributed equally to this work and share senior authorship.

***Correspondence:**
Barclay Jumet
barclay.jumet@rice.edu

Daniel J. Preston
djp@rice.edu

Keywords: Stacked-Sheet Lamination, Textiles, Pouch Motor, Mechanotherapy, Untethered, Intermittent Pneumatic Compression

Word Count: 4,891
Figures: 4
Tables: 0

Abstract

In 2020, cardiovascular diseases resulted in 25% of unnatural deaths in the United States. Treatment with long-term administration of medication can adversely affect other organs, and surgeries such as coronary artery grafts are risky. Meanwhile, sequential compression therapy (SCT) offers a low-risk alternative, but is currently expensive and unwieldy, and often requires the patient to be immobilized during administration. Here, we present a low-cost wearable device to administer SCT, constructed using a stacked lamination fabrication approach. Expanding on concepts from the field of soft robotics, textile sheets are thermally bonded to form pneumatic actuators, which are controlled by an inconspicuous and tetherless electronic onboard supply of pressurized air. Our open-source, low-profile, and lightweight (140 g) device costs $62, less than one-third the cost the least expensive alternative and one-half the weight of lightest alternative approved by the US Food and Drug Administration (FDA), presenting the opportunity to more effectively provide SCT to socioeconomically disadvantaged individuals.. Furthermore, our textile stacking method, inspired by conventional fabrication methods from the apparel industry, along with the lightweight fabrics used, allows the device to be worn more comfortably than other SCT devices. By reducing physical and financial encumbrances, the device presented in this work may better enable patients to treat cardiovascular diseases and aid in recovery from cardiac surgeries.

1. Introduction

Cardiovascular disease is the top global cause of unnatural deaths, and has accounted for the largest increase in deaths since the year 2000 (World Health Organization, 2020). Globally, there were over 420 million cases of cardiovascular disease in 2015, with the top three most widespread and severe arterial diseases being deep vein thrombosis (DVT), peripheral artery disease (PAD), and coronary artery disease (CAD) (Roth *et al.*, 2017). CAD, which is particularly deadly and more widespread than DVT and PAD, accounts for approximately one-third of all deaths in individuals over the age of 35 (Wilson, O'Donnell, and C.J., 2017). In addition to the death toll, cardiovascular diseases can debilitate survivors and have consequently forced millions of people to suffer from residual issues long after acute treatment. As for DVT, within 1 year of diagnosis, between 17–50% of cases lead to post-thrombotic syndrome, which is a chronic and potentially disabling condition (Kesieme and Kesieme, 2011). Furthermore, PAD (the third-leading cause of death associated with cardiovascular morbidity worldwide) is becoming increasingly common as the number of people diagnosed with PAD increased by 28.7% in low-to-middle-income countries and by 13.1% in high-income countries from 2000 to 2010 (Fowkes *et al.*, 2013). The inverse correlation between socioeconomic status and risk of cardiovascular disease is reflected in the higher-income countries as well, as evidenced by Steptoe et al. Their work corroborated that people of low socioeconomic status have a higher prevalence of risk factors for cardiovascular diseases (Steptoe *et al.*, 2006). The causes of these cardiovascular diseases include age, smoking, systolic blood pressure, serum total cholesterol, diabetes mellitus, and body mass index (Celermajer *et al.*, 2012). To avoid cardiovascular disease, most research suggests eating a balanced diet, being physically active, keeping a healthy weight, giving up smoking, reducing alcohol consumption, and keeping diabetes under control (Lonn and Yusuf, 1999).

Once a patient is diagnosed with cardiovascular disease, such as DVT, PAD, or CAD, the typical options for treatment to lower the risk of a significant cardiovascular event include (i) long-term use of medications, (ii) high-risk revascularization surgeries, and (iii) substantial lifestyle changes and structured exercise regimens (Gerhard-Herman *et al.*, 2017). Sequential compression therapy (SCT) also functions to lower the risk of a significant cardiovascular event and is recommended alongside the typical treatment options. Additionally, SCT during walking or rehabilitative sessions is significantly more effective in reducing the risk for cardiovascular disease than either exercise or SCT alone (Sakai *et al.*, 2021). Long-term medications are proven to be effective at addressing heart diseases, but they are often accompanied by side effects related to the patient's liver or kidneys. Besides medications, coronary bypass surgery can be an effective treatment; however, it is a high risk surgery and therefore is rarely performed, even on ideal candidates (Rodríguez-Olivares *et al.*, 2018). Even for patients who undergo major open-heart surgeries, there remains a period of time following the operation where they are at high risk of a significant cardiovascular event before full recovery. Given the limitations of these options, SCT stands out as an enticing complementary or alternative approach. SCT is a form of moderated mechanotherapy that can both preemptively relieve the symptoms of heart diseases and render post-operative aid to patients as they recover after surgeries. Depending on the patient's cardiovascular symptoms, different SCT regimens could be used in a hospital or at home. A literature review of SCT studies found that most regimens of SCT included multiple sessions lasting 45 minutes each; however, there are a range of regimens which showed effectiveness with sessions lasting three minutes to several hours (Phillips and Gordon, 2019). SCT shows promise as a treatment to cardiovascular diseases because it improves arterial blood flow in the limbs via mechanically pumping blood proximally, which leads to reductions in the risk factors for CAD (e.g., hypertension) by lessening the work needed by the heart to circulate blood (Labropoulos *et al.*, 2005). SCT can also prevent PAD-caused critical limb ischemia from worsening into acute limb ischemia, which often leads to amputation (Labropoulos *et al.*, 2005). Additionally, SCT is currently medically advised to help heal the heart if revascularization is performed to cure CAD (Maleti, 2016). Clinical data also suggest that after undergoing surgery to treat DVT, SCT lowers the risk of post-thrombotic syndrome by 60% (Gwozdz *et al.*, 2020). Therefore, SCT not only functions as a treatment for cardiovascular diseases, but also offers significant value in recovering from a cardiovascular surgery.

Unfortunately, conventional devices capable of performing SCT (Figure 1A) have numerous drawbacks that inhibit their effectiveness and accessibility as a treatment option for DVT, PAD, and CAD. These drawbacks include their bulkiness, immobility, and high cost. Often comprising cumbersome or tethered components, conventional SCT devices are heavy and uncomfortable, consequently limiting the user's mobility and shortening the duration of each session of SCT. Beyond the relatively superficial encumbrance of current devices, immobilization and shorter durations of SCT negatively impact the effectiveness of both the treatment of and recovery from DVT, PAD, and CAD (Zaleska, Olszewski and Durlik, 2014). Besides their physically limiting designs, the high costs associated with SCT devices are a significant disadvantage, specifically due to the inverse socioeconomic correlation with cardiovascular diseases. As shown in Figure 1B, the cost of renting a conventional SCT device can range from \$100 to \$500 over the course of a one-month treatment cycle, and buying one can cost over \$1000 (Figure 1B, Table S1). Compounding these income-related disparities, people of low socioeconomic status have statistically higher rates of the risk factors for DVT, PAD, and CAD, including smoking, adverse lipid profiles, abdominal adiposity, and inflammatory markers (Steptoe *et al.*, 2006). This fact, considered alongside the often-prohibitive cost of SCT, indicates that populations who need SCT the most are least likely to be able to afford it. Because SCT offers unique value in the treatment of ever-prevalent cardiovascular diseases, an affordable and more mobile SCT device is necessary.

In developing a portable and controllable SCT alternative, safety at the interface between humans and devices represents a critical concern that can be solved by inputs of risk-aware human models into robotic controllers (Kwon *et al.*, 2020), the use of non-anthropomorphic designs (Tagliamonte *et al.*, 2013), or making the devices intrinsically safe via soft robotic concepts. Soft robots lessen the safety risk associated with traditional (i.e., rigid) robots and are becoming especially beneficial in the design process for applications that regularly interface with humans. While textiles, a subset of sheet-based materials, are the least used category of soft materials in soft robotic components (Jumet, Bell, *et al.*, 2022), they offer unique advantages in actuation (due to their ability to be designed for both strength and compliance) and in human-machine interfaces (because textiles are already ubiquitous in interfacing directly with humans). By leveraging their pliable geometry, the functions of sheet-based devices are diverse, ranging from oscillating actuators (Lee *et al.*, 2022) to instability driven locomotion (Nagarkar *et al.*, 2021). Going further, sheet-based devices made from textiles have been demonstrated in useful soft systems, such as functionally complete logic control (Rajappan *et al.*, 2022) and power generation from walking (Shveda *et al.*, 2022). Additionally, prior work in soft robotics has shown that textile-based wearable devices represent a promising solution for low-cost, untethered, and lightweight devices that apply forces to the body (Sanchez, Walsh and Wood, 2021). Mechanotherapy is a well-suited application for soft roboticists because the intrinsic benefits of soft robotics, such as pliable human-device interfaces, are leveraged toward an important application: the promotion of muscle and bone tissue via mechanotransduction (Khan and Scott, 2009). For example, Payne et al. designed and tested a low-cost, low-profile, soft wearable device for muscle regeneration via mechanotherapy (Payne *et al.*, 2018). More recently, Preston et al. demonstrated an inflatable mechanotherapy leg wrap as an application for a soft ring oscillator (Preston *et al.*, 2019). Additionally, low-cost wearable devices, including a mechanotherapy device, were explored by

Sanchez et al. as applications for smart thermally actuating textiles (STATs). These STATs were constructed by leveraging stacked fabrication of 2D sheets, to which textile devices lend themselves well (Sanchez *et al.*, 2020). Beyond mechanotherapy, several authors have explored soft wearables as pneumatically actuated haptic devices that provide tactile (e.g., squeeze) cues to the body (Raitor, 2017; Agharese *et al.*, 2018; Wu and Culbertson, 2019; Goetz, Owusu-Antwi and Culbertson, 2020; Jumet, Zook, *et al.*, 2022). However, prior literature has not focused specifically on the development and characterization of a device to solve the problem of inaccessible SCT.

In this paper, we present a low-cost, soft, wearable device for SCT to provide comparable pressure delivery and functionality to the state of the art in a comfortable, mobile, low-profile, and inexpensive manner that consequently has a low impact on the user's lifestyle. Differing in design from the targeted mechanotherapy devices which use one sleeve composed of a series of several large pouches that inflate inward to provide a compressive force (Payne *et al.*, 2018), the presented SCT device has three individual straps, each composed of low-profile serial pouches called "pouch motors" (Mettam, 1962; Sanan, Lynn and Griffith, 2014; Yang *et al.*, 2016) that wrap around the limb and constrict circumferentially to provide an inward pressure, in doing so providing the medically advised level of pressure and duration of compression necessary to conduct SCT. While more general compression sleeves have represented a common application space for soft robotic wearables in the literature (Payne *et al.*, 2018; Preston *et al.*, 2019; Sanchez *et al.*, 2020; Jumet, Zook, *et al.*, 2022), we instead focus in this work on the design and modeling of force transduced in the form of Laplace pressure (de Gennes, Brochard-Wyart and Quéré, 2004), where circumferential force applied by a pouch motor is converted to normal pressure applied to the leg in our mechanotherapeutic device. As a potential solution to a common yet previously expensive problem, our device exhibits economic competitiveness at a cost of $62 and can be made from commercially available parts that are comfortable and (financially and physically) less inhibiting to the patient. An additional benefit for the presented mobile SCT is the small form factor of our device, which adds negligible weight and allows sessions of SCT to be easily started and stopped, which significantly improves quality of life. Even in cases where patients who are prescribed SCT struggle with getting in and out of bed and may require an attendant to put on the SCT device, our approach allows for a simpler and more comfortable approach than most. Furthermore, we demonstrate that our soft device performs comparably to existing commercial counterparts and can operate across the medically advised range of pressures for successful SCT.

2. Materials and Methods

2.1. Fabrication

The device presented in this work relies on a two-dimensional (2D) stacked fabrication process. This process is advantageous due to its simplicity, which lends itself to inexpensive batch fabrication that is possible to perform in a do-it-yourself (DIY) manner, further enabling potential adoption by economically disadvantaged users. The 2D stacking technique enables the operational principle of the device: pouch motors (Mettam, 1962; Sanan, Lynn and Griffith, 2014; Yang *et al.*, 2016). The pouch motor's transition from planar rectangular sections to 3D cylindrical chambers via pneumatic inflation allows the transduction of applied pressure within the pouches to lateral tensile force by decreasing the effective length of the once-planar sections (Figure 1C). When the pouch motors are fashioned into straps which connect around the leg, the decrease in effective length of the straps becomes a decrease in the circumference of the now-circular strap. The Laplace pressure relationship indicates that circumferential force around a circular cross section induces a pressure directed radially inward, which is the essential mode of actuation for sequential compression therapy (Figure 1D).

We manufacture the SCT device by cutting—either with a laser cutter or other conventional fabric cutting techniques—three 2D layers: two outer layers of heat-sealable textile (nylon taffeta infused with thermoplastic polyurethane [TPU] [Seattle Fabrics, FHST] on the inner sides, which bond together), and one intermediate non-stick layer (parchment paper). The non-stick layer contains three sets of serially connected 2D rectangles, which ultimately define the arrays of 3D pneumatic pouches comprising each pouch motor when inflated. We insert the non-stick layer between the two heat-sealable layers and bond the stacked layers with a heat press for 30 seconds at 345 kPa and 200° C as shown in Figure 2A. Alternatively, if fabricating the device in a DIY manner, one could replace the heat press with an iron or another source of pressure and heat. After cutting and heat pressing the three layers, the functional portion of the device is complete, comprising three straps that wrap around the leg in the transverse plane and connect perpendicularly to a common section which maintains the positions of the straps relative to each other. This perpendicular section is oriented along the distal-proximal axis of the leg.

The final 2D intermediate geometry for each strap includes 5 pouches, each with a pouch length of 3 cm and a pouch width of 3 cm (both of which were empirically derived due to the indeterminant angle of the pouch (θ) as later discussed in Section 2.2). Long, thin channels of the nonstick layer connect each of the three sets of pouches to the proximal (i.e., “top”) end of the common section. Additionally, we secured Luer lock fittings to the inlets of the serial arrays of pouches by applying heat to the TPU around the fittings, shrinking the TPU coating to form around them, and then applying epoxy (J-B Weld, Plastic Bonder 50139) to the fittings. Lastly, we attached adhesive-backed (or alternatively, sewn-in) hook-and-loop fasteners to each strap such that it could be secured snugly and was able to fit comfortably on various diameters of legs as well as the different diameters encountered along the axis of a particular leg. The fabrication process as well as the geometry of the serial pouches and their respective inlets that make up the three straps of the SCT device are shown in Figure 2A.

We designed an electronic control system to regulate the supplied pressure and to sequence the timing and actuation of each strap. The primary electrical components consist of an Arduino Nano IOT 33, a pneumatic micropump (Skoocom, SC3101PM) with a flow rate of 205 mL/min, three miniature Lee Company pneumatic valves (LHDA0531115H), and two 20-mm x 18-mm x 10-mm, 2-cell, 120-mAh, 7.4-V LiPo batteries. By sending 3.3-V signals to specific negative-positive-negative (NPN) transistors, the device can selectively power the micropump and any of the three valves. When simultaneously supplying power to the micropump and a particular valve, pressure is supplied to the strap associated with the valve, allowing for compression to be applied to the leg beneath that strap (Figure 2B). SCT is achieved by sequentially powering the valves associated with straps A, B, and C, which peristaltically assists proximal blood flow from the leg (Figure 1C–D). The device can operate for 53 minutes, which is enough time for a session of SCT (Phillips and Gordon, 2019). Larger batteries could enable multiple sessions. Furthermore, the power consumption is 2 W, and previous research provided a textile-based energy harvesting device that could supply an output of 3 W showing promise for future work (Shveda *et al.,* 2022).

Furthermore, to generalize the device’s capabilities for almost any patient, the controller must be able to adjust the supply pressure based on the diameter of the leg because of the circumference’s inverse relationship with the applied pressure, as prescribed by the Laplace pressure formula (described in detail in the next section). We accomplished this generalization by including an easy-to-use mechanical adjustment knob for each strap, which a doctor or patient would be able to set according to a measurement of the leg’s diameter at the location of each strap. Based on the settings of these adjustment knobs, the Arduino modifies the pressure in each strap using pulse width modulation by cycling the strap's respective valve on and off rapidly. Through this process, most patients would be able to use the device to receive sequential compression therapy tailored for their particular anatomical dimensions and needs.

2.2. Analytical Modeling

As described above, our SCT device contains three straps, where each one of the straps contains a series of pouches and can thus be modeled as a pouch motor (Niiyama *et al.*, 2015). Here, we adopted and modified the model from Niiyama et al. for each pouch motor to relate the pneumatic input pressure, P_{pouch}, to the in-plane pouch motor force, F_{strap}, and ultimately to the induced Laplace pressure applied to the leg. We represent the force of a given strap, F_{strap}, in Eq. 1, where L_0 and L_1 are the length and width, respectively, of one pouch within a strap, and θ is the tangential angle of the textile sheet at the vertex of each pouch that characterizes the degree of lenticular transition of the pouch from a planar rectangle to a 3D cylindrical shape (Figure 1C). For a given contraction of the strap around a rigid or near-rigid body (in this case, the leg), θ remains constant, and therefore F_{strap} exhibits a linear relationship with P_{pouch}, as evidenced in Figure 3A by the constant slope describing the amount of contraction force, denoted here by $\mathrm{L_0L_1}\cos(\theta)\ \theta^{-1}$, where θ is approximately constant.

$$F_{\text{strap}} = L_0 L_1 \frac{cos(\theta)}{\theta} P_{\text{pouch}} \qquad \text{Eq. (1)}$$

We relate F_{strap} and the pressure felt on the leg, P_{L}, using the relationship of Laplace pressure. When the strap is wrapped around the leg, the tensile force within a strap effectively acts as a circumferential "surface tension" (Figure 1D). In the field of interfacial phenomena, the Young-Laplace equation describes the Laplace pressure as a function of surface tension, γ, and the radius, r, which in this case corresponds to the leg, approximated as a cylinder with only one principal curvature (de Gennes, Brochard-Wyart and Quéré, 2004). The surface tension is a force per perpendicular unit length (L_1). Following this analogy, a positive surface tension induces an inward Laplace pressure (P_{L}) on the leg as described in Eq. 2, where r is the local radius of the leg beneath the strap.

$$P_{\text{L}} = \frac{\gamma}{r} = \frac{F_{\text{strap}}}{L_1 r} \qquad \text{Eq. (2)}$$

We experimentally measured the force applied to the leg using a small, flexible force sensor as detailed in the Supplementary Material. This force, F_{leg}, can be related to P_{L} through Eqs. 3 and 4, where A_{eff} is the effective surface area of the force sensor determined using a factor of α to correct for the geometric stress concentration on the sensor (we used $\alpha = 2.4$ in this work).

$$P_{\text{L}} = \frac{F_{leg}}{A_{\text{eff}}} \qquad \text{Eq. (3)}$$

$$A_{\text{eff}} = \alpha A_{\text{sensor}} \qquad \text{Eq. (4)}$$

Combining all above equations, we relate the pressure applied to the outer surface of the leg, P_{L}, to the pressure input in a given strap, P_{pouch}, of the SCT device with Eq. 5.

$$P_{\text{L}} = \frac{L_0 * \frac{cos(\theta)}{\theta}}{r} * P_{\text{pouch}} \qquad \text{Eq. (5)}$$

This linear model (seen in Figure 3A–B) highlights the necessity of controlling P_{pouch} to set P_{L}, which we achieved through varying the duty cycle, DC, of our micropumps while measuring F_{leg}. The relationship between F_{leg} and DC within our operational range can be fitted with Eq. 6, where C_1 and C_2 are constant calibration factors for the micropump used in our device.

$$F_{leg} = C_1 * DC + C_2 \qquad \text{Eq. (6)}$$

3. Results

Using a universal testing machine (Instron, 68SC-2), we quantified the tensile force, F_{strap}, generated as a function of the input pneumatic pressure, P_{pouch}. Within the operational range, the data agree with the expected linear relation between F_{strap} and P_{pouch}. The angle of a given pouch, θ, has an implicit relationship with F_{strap} but can be obtained through a Taylor series expansion. However, due to the observed linear relationship between force and pressure, further derivation is unnecessary because θ (which correlates to the contraction of the strap) remains approximately constant throughout the entire range of P_{pouch}, matching our expectation that the leg acts approximately as a rigid body. Therefore, we performed a linear regression to find the relationship between F_{strap} and P_{pouch} based on Eq. 1 with a constant operational θ (i.e., contraction) for the device (Figure 3A). The θ that provides a solution for this particular slope is 46.0°.

We tested the device on an anatomically proportionate mannequin leg wrapped with a layer of silicone elastomer (Smooth-On, Dragon Skin™ 10 Very Fast) to emulate cutaneous and subcutaneous tissue, whereas the plastic portion of the mannequin emulated the more rigid musculoskeletal tissue underneath; we placed three force-sensing resistors (Interlink Electronics, FSR 402) between the elastomer and the leg. With the known input pneumatic pressure and geometry of each inflated strap, the sensors measured the applied force (F_{leg}) exerted on the leg by each strap. While the position of the pouch motor does have some impact on the force, the effect is significantly mitigated by the elastomer wrap which distributes the force. On a human, the compliance of the cutaneous and subcutaneous tissue would act similarly. We experimentally determined that the maximum force difference due to orientation of the pouches relative to the sensor was less than 15.5%. However, the internal plastic component of the mannequin's leg provides enough structural integrity to act as a rigid body, relegating any effect of preload (i.e., tightness) when donning the device as negligible. Furthermore, as shown in Figure 3B, the empirical data from these sensors validate our linearized model based on Laplace pressure, suggesting reasonable reliance on the strap to transform P_{pouch} into F_{leg} (and therefore, to apply P_{L}) in a controlled manner.

Additionally, we measured several forces on the leg created by varying the duty cycles, using the same experimental setup as before. These results show that for a specified leg diameter, different steady-state F_{leg} (and P_{L}) could be achieved by varying the duty cycle (Figure 3C). Having observed that P_{pouch} varies linearly with respect to $DC,$ we were able to perform another regression to find the approximate relationship between the steady-state F_{leg} and DC (Figure 3D). This relationship was used as a calibration curve for low-cost control of the F_{leg} (and, correspondingly, P_{L}) exerted by each strap; that is, one can simply calculate the input DC required for a desired F_{leg} or P_{L} (Eq. 6).

To ensure all three straps exert the same amount of pressure on the leg despite the diameter of the leg varying along its longitudinal axis, we controlled the actuation of the device with separate duty cycles for each strap (Figure 4B). Using this method of open-loop control, we were able to tailor the forces with the built-in adjustment knobs and consequently set the induced peak Laplace pressures applied to the leg for each strap independently (Figure 4C–D), given that each strap enclosing a leg portion with different radii requires different duty cycles to reach the same Laplace Pressure (Eq. 5-6). Transferring the control and strap setup to a human leg (Figure 4A), we reproduced the controlled sequential compression results (Figure 4D). With the recorded applied force divided by the effective area of the sensor (1.77 cm^2) equating to 90 mm Hg and 50 mm Hg (Figure 4C and 4D, respectively), we show that the pressure applied by the straps is adjustable and that the device performs in accordance with the medical guidelines of 40–120 mm Hg of induced pressure for SCT (Zaleska *et al.*, 2013). Moreover, the device achieves its target applied pressure in 9.7 s (Figure 4B-D), which satisfies SCT requirements as it is suggested for pressure to be applied over a duration of 50 s per strap (Zaleska *et al.*, 2013). Furthermore, even when unregulated, the device produce a maximum applied pressure of only 450 mm Hg (which results in 25 N applied to the leg of the wearer, Figure 4B), thus applying less force than a mechanotherapy device described in prior work which reported no adverse effects (Payne *et al.*, 2018), and therefore suggesting a level of safety in the event that our controller were to be inactivated. In this manner, we operated our device independent of any physical tether and were able to perform tailored mechanotherapy on a human leg without immobilization or interruption of day-to-day activities following only one initial open-loop calibration step (which could be performed by care providers in a clinical setting) using the DC adjustment knobs through measuring the leg and calculating the duty cycle needed; as such, we have demonstrated the efficacy of the device in a scenario that is more reasonable for a patient than current devices that require a physically encumbering tether or a financially burdening investment.

4. Discussion

From data gathered via our benchtop rig and on a human user, we have shown that our SCT device can supply the necessary pressures and intervals of inflation needed for sequential compression therapy at less than one third of the cost of the most affordable FDA-approved SCT device. We demonstrate qualitative and quantitative improvements over the state of the art, which have significant implications for three major reasons. Firstly, the mobility and wearability of this device are superior to conventional devices and thus allow SCT to be an even more viable and practical option for treatment of cardiovascular diseases than it has been in the past. Secondly, the improvement of a non-pharmaceutical treatment for cardiovascular disease is remarkable, as non-pharmaceutical treatment options do not have significant side effects relative to medical and surgical approaches yet are currently limited to only two options, structured exercise or SCT (Gerhard-Herman *et al.*, 2017). Lastly, reducing the cost of SCT devices through the aforementioned fabrication approach stemming from soft robotics is particularly important because people of low socioeconomic status have more risk factors for cardiovascular diseases, and this low-cost device may provide more accessible treatment for those who need it. It has also been shown that devices of similar textile structures and materials to our device are machine washable and remain functional after 20,000 cycles of actuation, *which is equivalent to 50,000 minutes of SCT for our device, making our device ideal for wearable purposes* (Rajappan *et al.*, 2022). Furthermore, the files used to create all parts of the device have been provided in the Supporting Material to allow open-access fabrication.

Future work for this device could attempt to further improve the advantages that we have demonstrated. The low profile and portability of the device can be further iterated upon by integrating the presented device directly into a piece of clothing. For example, sewing the straps of the device into (or underneath) a pant leg would enable the device to be wearable like conventional garments yet still provide SCT in an inconspicuous and comfortable manner. The implementation of textile-based energy harvesting or logic control could enable the device to be made solely from textile materials, ensuring an entirely soft (and washable) device (Shveda *et al.*, 2022; Rajappan *et al.*, 2022). The system could also be further developed to deliver SCT more precisely in an automatic manner by using closed-loop control (Payne *et al.*, 2018; Sanchez *et al.*, 2020).

Beyond the advantages for patients with cardiovascular issues, the presented device also has significant implications for the field of soft robotics because it is a soft device with a clear and important relevance to the medical industry. Previously, Cianchetti et al. asserted that the field of soft robotics is appropriate for the design of biomedical devices (Cianchetti *et al.*, 2018), and Rose and O'Malley explored a soft device which promotes functional dexterity (Rose and O'Malley, 2019). As the field of soft robotics continues to grow within academic research (Jumet, Bell, *et al.*, 2022), it is important that it grows in industry and commercialization as well; this work represents a proof of concept of a soft robotic device which can be effectively applied outside of benchtop testing and exhibits performance comparable to conventional commercial devices (Gu *et al.*, 2021; Rothemund *et al.*, 2021). Furthermore, the simplicity of our approach, in part due to its reliance on soft robotic concepts, enables it to be assembled as an open-source device that is highly accessible, adding another example of open-source robotics—similar to prior work that developed an exoskeleton test bed (Baskaran *et al.*, 2021)—to the literature. Our work thus serves as an example of a concept from soft robotics that can be effectively and pragmatically applied to solve critical problems, such as addressing the inaccessibility for the treatment of cardiovascular diseases by easing the suffering of economically disadvantaged people living with cardiovascular diseases.

Permission to Reuse and Copyright

Conflict of Interest

The authors declare that the research was conducted in the absence of any commercial or financial relationships that could be construed as a potential conflict of interest.

Author Contributions

MS, MZ, and DJP designed the experiments, and MS and MZ performed the experiments and collected and analyzed the data. BJ optimized the fabrication process. MS and MZ wrote the manuscript with feedback from BJ and DJP. All authors have read and approved the final manuscript. BJ and DJP supervised the work.

Funding

This research was supported by scholarships provided by the Hispanic Scholarship Fund and by the Sustaining Excellence in Research (SER) Scholars program. This research was also supported by the National Science Foundation (NSF) under Grant No. 2144809 and the NSF Graduate Research Fellowship under Grant No. 1842494. Any opinions, findings, and conclusions or recommendations expressed in this material are those of the author(s) and do not necessarily reflect the views of the National Science Foundation

Acknowledgments

Dr. Anoop Rajappan generously aided the authors with design of experiments and data collection.

References

Agharese, N. *et al.* (2018) 'HapWRAP: Soft Growing Wearable Haptic Device', in *2018 IEEE International Conference on Robotics and Automation (ICRA)*. Brisbane, QLD: IEEE, pp. 5466–5472. Available at: https://doi.org/10.1109/ICRA.2018.8460891.

Baskaran, A. *et al.* (2021) 'An Anthropomorphic Passive Instrumented Hand for Validating Wearable Robotic Systems', in *2021 IEEE/ASME International Conference on Advanced Intelligent Mechatronics (AIM)*. Delft, Netherlands: IEEE, pp. 134–139. Available at: https://doi.org/10.1109/AIM46487.2021.9517589.

Cardinal Health 'PlasmaFlow Portable Compression Device'. Available at: https://www.cardinalhealth.com/en/product-solutions/medical/compression/plasmaflow-portable-compression.html.

Cardinal Health 'Kendall SCD 700 Series Controller'. Available at: https://www.cardinalhealth.com/en/product-solutions/medical/compression/kendall-scd-compression-system/kendall-scd-700-series-controller.html.

Celermajer, D.S. *et al.* (2012) 'Cardiovascular Disease in the Developing World', *Journal of the American College of Cardiology*, 60(14), pp. 1207–1216. Available at: https://doi.org/10.1016/j.jacc.2012.03.074.

Cianchetti, M. *et al.* (2018) 'Biomedical applications of soft robotics', *Nature Reviews Materials*, 3(6), pp. 143–153. Available at: https://doi.org/10.1038/s41578-018-0022-y.

Fowkes, F.G.R. *et al.* (2013) 'Comparison of global estimates of prevalence and risk factors for peripheral artery disease in 2000 and 2010: a systematic review and analysis', *The Lancet*, 382(9901), pp. 1329–1340. Available at: https://doi.org/10.1016/S0140-6736(13)61249-0.

de Gennes, P.-G., Brochard-Wyart, F. and Quéré, D. (2004) ‘Capillarity: Deformable Interfaces’, in P.-G. de Gennes, F. Brochard-Wyart, and D. Quéré (eds) *Capillarity and Wetting Phenomena: Drops, Bubbles, Pearls, Waves*. New York, NY: Springer, pp. 1–31. Available at: https://doi.org/10.1007/978-0-387-21656-0_1.

Gerhard-Herman, M.D. *et al.* (2017) ‘2016 AHA/ACC Guideline on the Management of Patients with Lower Extremity Peripheral Artery Disease: Executive Summary’, *Vascular Medicine*, 22(3), pp. NP1–NP43. Available at: https://doi.org/10.1177/1358863X17701592.

Goetz, D.T., Owusu-Antwi, D.K. and Culbertson, H. (2020) ‘PATCH: Pump-Actuated Thermal Compression Haptics’, in *2020 IEEE Haptics Symposium (HAPTICS)*. Crystal City, VA, USA: IEEE, pp. 643–649. Available at: https://doi.org/10.1109/HAPTICS45997.2020.ras.HAP20.32.c4048ec3.

Gu, G. *et al.* (2021) ‘A soft neuroprosthetic hand providing simultaneous myoelectric control and tactile feedback’, *Nature Biomedical Engineering*, pp. 1–10. Available at: https://doi.org/10.1038/s41551-021-00767-0.

Gwozdz, A.M. *et al.* (2020) ‘Post-thrombotic Syndrome: Preventative and Risk Reduction Strategies Following Deep Vein Thrombosis’, *Vascular and Endovascular Review*, 3, p. e15. Available at: https://doi.org/10.15420/ver.2020.15.

Jumet, B., Bell, M.D., *et al.* (2022) ‘A Data-Driven Review of Soft Robotics’, *Advanced Intelligent Systems*, 4(4), p. 2100163. Available at: https://doi.org/10.1002/aisy.202100163.

Jumet, B., Zook, Z.A., *et al.* (2022) ‘A Textile-Based Approach to Wearable Haptic Devices’, in *2022 IEEE 5th International Conference on Soft Robotics (RoboSoft)*. Edinburgh, United Kingdom: IEEE, pp. 741–746. Available at: https://doi.org/10.1109/RoboSoft54090.2022.9762149.

Kesieme and Kesieme (2011) ‘Deep vein thrombosis: a clinical review’, *Journal of Blood Medicine*, p. 59. Available at: https://doi.org/10.2147/JBM.S19009.

Khan, K.M. and Scott, A. (2009) ‘Mechanotherapy: how physical therapists’ prescription of exercise promotes tissue repair’, *British Journal of Sports Medicine*, 43(4), pp. 247–252. Available at: https://doi.org/10.1136/bjsm.2008.054239.

Kwon, M. et a*l.* (2020) ‘When Humans Aren’t Optimal: Robots that Collaborate with Risk-Aware Humans’, in *Proceedings of the 2020 ACM/IEEE International Conference on Human-Robot Interaction*. Cambridge United Kingdom: ACM, pp. 43–52. Available at: https://doi.org/10.1145/3319502.3374832.

Labropoulos, N. *et al.* (2005) ‘Hemodynamic effects of intermittent pneumatic compression in patients with critical limb ischemia’, *Journal of Vascular Surgery*, 42(4), pp. 710–716. Available at: https://doi.org/10.1016/j.jvs.2005.05.051.

Lee, W.-K. *et al.* (2022) ‘A buckling-sheet ring oscillator for electronics-free, multimodal locomotion’, *Science Robotics*, 7(63), p. eabg5812. Available at: https://doi.org/10.1126/scirobotics.abg5812.

Lonn, E.M. and Yusuf, S. (1999) ‘Emerging approaches in preventing cardiovascular disease’, *BMJ*, 318(7194), pp. 1337–1341. Available at: https://doi.org/10.1136/bmj.318.7194.1337.

Maleti, O. (2016) ‘Compression after vein harvesting for coronary bypass’, *Veins and Lymphatics*, 5(1). Available at: https://doi.org/10.4081/vl.2016.5989.

Mettam, A.R. (1962) ‘Inflatable Servo Actuators’, *Aeronautical Research Council, Ministry of Aviation*, C. P. No. 671.

Nagarkar, A. *et al.* (2021) ‘Elastic-instability–enabled locomotion’, *Proceedings of the National Academy of Sciences*, 118(8), p. e2013801118. Available at: https://doi.org/10.1073/pnas.2013801118.

Niiyama, R. *et al.* (2015) ‘Pouch Motors: Printable Soft Actuators Integrated with Computational Design’, *Soft Robotics*, 2(2), pp. 59–70. Available at: https://doi.org/10.1089/soro.2014.0023.

Payne, C.J. *et al.* (2018) ‘Force Control of Textile-Based Soft Wearable Robots for Mechanotherapy’, in *2018 IEEE International Conference on Robotics and Automation (ICRA)*. Brisbane, QLD: IEEE, pp. 5459–5465. Available at: https://doi.org/10.1109/ICRA.2018.8461059.

Phillips, J.J. and Gordon, S.J. (2019) ‘Intermittent Pneumatic Compression Dosage for Adults and Children with Lymphedema: A Systematic Review’, *Lymphatic Research and Biology*, 17(1), pp. 2–18. Available at: https://doi.org/10.1089/lrb.2018.0034.

Preston, D.J. *et al.* (2019) ‘A soft ring oscillator’, *Science Robotics*, 4(31), p. eaaw5496. Available at: https://doi.org/10.1126/scirobotics.aaw5496.

Raitor, M. (2017) ‘WRAP: Wearable, Restricted-Aperture Pneumatics for Haptic Guidance’, in. Singapore: 2017 IEEE International Conference on Robotics and Automation (ICRA).

Rajappan, A. *et al.* (2022) ‘Logic-enabled textiles’, *Proceedings of the National Academy of Sciences*, 35(119), p. e2202118119. Available at https://www.pnas.org/doi/10.1073/pnas.2202118119

Rodríguez-Olivares, R. *et al.* (2018) ‘Identification of candidates for coronary artery bypass grafting admitted with STEMI and Multivessel Disease’, *Cardiovascular Revascularization Medicine*, 19(6), pp. 21–26. Available at: https://doi.org/10.1016/j.carrev.2018.06.007.

Rose, C.G. and O’Malley, M.K. (2019) ‘Hybrid Rigid-Soft Hand Exoskeleton to Assist Functional Dexterity’, *IEEE Robotics and Automation Letters*, 4(1), pp. 73–80. Available at: https://doi.org/10.1109/LRA.2018.2878931.

Roth, G.A. *et al.* (2017) ‘Global, Regional, and National Burden of Cardiovascular Diseases for 10 Causes, 1990 to 2015’, *Journal of the American College of Cardiology*, 70(1), pp. 1–25. Available at: https://doi.org/10.1016/j.jacc.2017.04.052.

Rothemund, P. *et al.* (2021) ‘Shaping the future of robotics through materials innovation’, *Nature Materials*, 20(12), pp. 1582–1587. Available at: https://doi.org/10.1038/s41563-021-01158-1.

Sakai, K. *et al.* (2021) ‘Effects of intermittent pneumatic compression on femoral vein peak venous velocity during active ankle exercise’, *Journal of Orthopaedic Surgery*, 29(1), p. 230949902199810. Available at: https://doi.org/10.1177/2309499021998105.

Sanan, S., Lynn, P.S. and Griffith, S.T. (2014) ‘Pneumatic Torsional Actuators for Inflatable Robots’, *Journal of Mechanisms and Robotics*, 6(3), p. 031003. Available at: https://doi.org/10.1115/1.4026629.

Sanchez, V. *et al.* (2020) ‘Smart Thermally Actuating Textiles’, *Advanced Materials Technologies*, 5(8), p. 2000383. Available at: https://doi.org/10.1002/admt.202000383.

Sanchez, V., Walsh, C.J. and Wood, R.J. (2021) ‘Textile Technology for Soft Robotic and Autonomous Garments’, *Advanced Functional Materials*, 31(6), p. 2008278. Available at: https://doi.org/10.1002/adfm.202008278.

Shveda, R.A. *et al.* (2022) ‘A Wearable Textile-Based Pneumatic Energy Harvesting System for Assistive Robotics’, *Science Advances*, 34(8), p. eabo2418. Available at: https://www.science.org/doi/10.1126/sciadv.abo2418

Steptoe, A. *et al.* (2006) ‘Socioeconomic status, pathogen burden and cardiovascular disease risk’, *Heart*, 93(12), pp. 1567–1570. Available at: https://doi.org/10.1136/hrt.2006.113993.

Tagliamonte, N.L. *et al.* (2013) ‘Human-robot interaction tests on a novel robot for gait assistance’, in *2013 IEEE 13th International Conference on Rehabilitation Robotics (ICORR)*. Seattle, WA: IEEE, pp. 1–6. Available at: https://doi.org/10.1109/ICORR.2013.6650387.

Wilson, O’Donnell, P.W.F., and C.J. (2017) ‘Epidemiology of Chronic Coronary Artery Disease’, in *Chronic Coronary Artery Disease: A Companion to Braunwald’s Heart Disease*. 1st edn. Elsevier.

World Health Organization (2020) *The Top 10 Causes of Death [Fact Sheet]*. World Health Organization. Available at: https://www.who.int/news-room/fact-sheets/detail/the-top-10-causes-of-death.

Wu, W. and Culbertson, H. (2019) ‘Wearable Haptic Pneumatic Device for Creating the Illusion of Lateral Motion on the Arm’, in *2019 IEEE World Haptics Conference (WHC)*. Tokyo, Japan: IEEE, pp. 193–198. Available at: https://doi.org/10.1109/WHC.2019.8816170.

Yang, D. *et al.* (2016) ‘Buckling Pneumatic Linear Actuators Inspired by Muscle’, *Advanced Materials Technologies*, 1(3), p. 1600055. Available at: https://doi.org/10.1002/admt.201600055.

Zaleska, M. *et al.* (2013) ‘Pressures and Timing of Intermittent Pneumatic Compression Devices for Efficient Tissue Fluid and Lymph Flow in Limbs with Lymphedema’, *Lymphatic Research and Biology*, 11(4), pp. 227–232. Available at: https://doi.org/10.1089/lrb.2013.0016.

Zaleska, M., Olszewski, W.L. and Durlik, M. (2014) ‘The Effectiveness of Intermittent Pneumatic Compression in Long-Term Therapy of Lymphedema of Lower Limbs’, *Lymphatic Research and Biology*, 12(2), pp. 103–109. Available at: https://doi.org/10.1089/lrb.2013.0033.

Data Availability Statement

The datasets used in this study can be found in the Supplementary Material.

Figure Captions

Figure 1. (**A**) Tethered and bulky conventional SCT devices limit the patient's mobility; (**B**) price comparisons are shown of the commercially FDA-approved SCT devices relative to our device; (**C**) each strap of the presented device contains a pouch motor that applies a linear force (F_{strap}) based on the dimensions L_0 and L_1, the pressure P_{pouch}, and each constituent pouch's tangential angle (θ) relative to the plane of the device. Each of these straps are sequentially activated causing a contraction that constricts around the leg to apply an inward pressure; (**D**) the presented device performs sequential compression, using the same mechanism by which surface tension induces an analogous Laplace pressure (P_L), starting at the distal end of the limb and progressing proximally toward the heart.

Figure 2. (**A**) Fabrication process includes cutting, aligning, heat pressing, and adding pneumatic components. (**B**) Schematic of the device and controller shows the electrical connections that power the micropump valves and the pneumatic connections to the straps; here, the controller activates valve A, enabling pressure to increase within strap A.

Figure 3. (**A**) the linear force (F_{strap}) of each strap at different input pressures (P_{pouch}), which is modeled linearly within our operational range of pressures. The error bars in Figure 3A are fixed at 2.5kpa, which is the experimentally observed fluctuation of our supplied pressure, measured by the pressure gauge during the contractile force testing in the universal testing machine. The error bars in Figure 3B are fixed at 1N, which is the error range of the force sensor's raw data that we averaged to obtain the final single data point; (**B**) The force on the leg (F_{leg}) at radius, r, is measured, equated to the induced Laplace pressure (P_{L}), and plotted against the model from Eq. 5; (**C**) F_{leg} over time of one strap at different DC is measured and plotted; (**D**) plotting the steady state F_{leg} in Figure 3C versus DC, the experimenters obtained the control calibration curve for the presented device.

Figure 4. (**A-i**) The mannequin leg wears the SCT device, with a sensor measuring the F_{leg} between the leg and the Dragon Skin elastomer; (**A-ii**) the same setup is attached to human leg with a thigh-mounted electropneumatic controller containing the micropump, solenoid valves, and microcontroller. (**B**) In the unregulated regime, all three straps pressurize to the same P_{pouch}, and strap A (wrapped around a portion of the leg that has a smaller diameter) exerts significantly greater F_{leg}, which agrees with the Laplace force model in Eq. 5. Under open-loop control, the duty cycle controls all three straps with different magnitudes of P_{pouch} in correspondence with their particular diameters, thereby producing the same F_{leg} along the leg. (**C**) All straps exert the same P_{L} with regulated duty cycles, achieving nearly 100 mm Hg on the mannequin. (**D**) Device delivers SCT on the human leg at 50 mm Hg, falling within the suggested range of pressures of 40–120 mm Hg (Zaleska *et al.*, 2013).

Figure 1

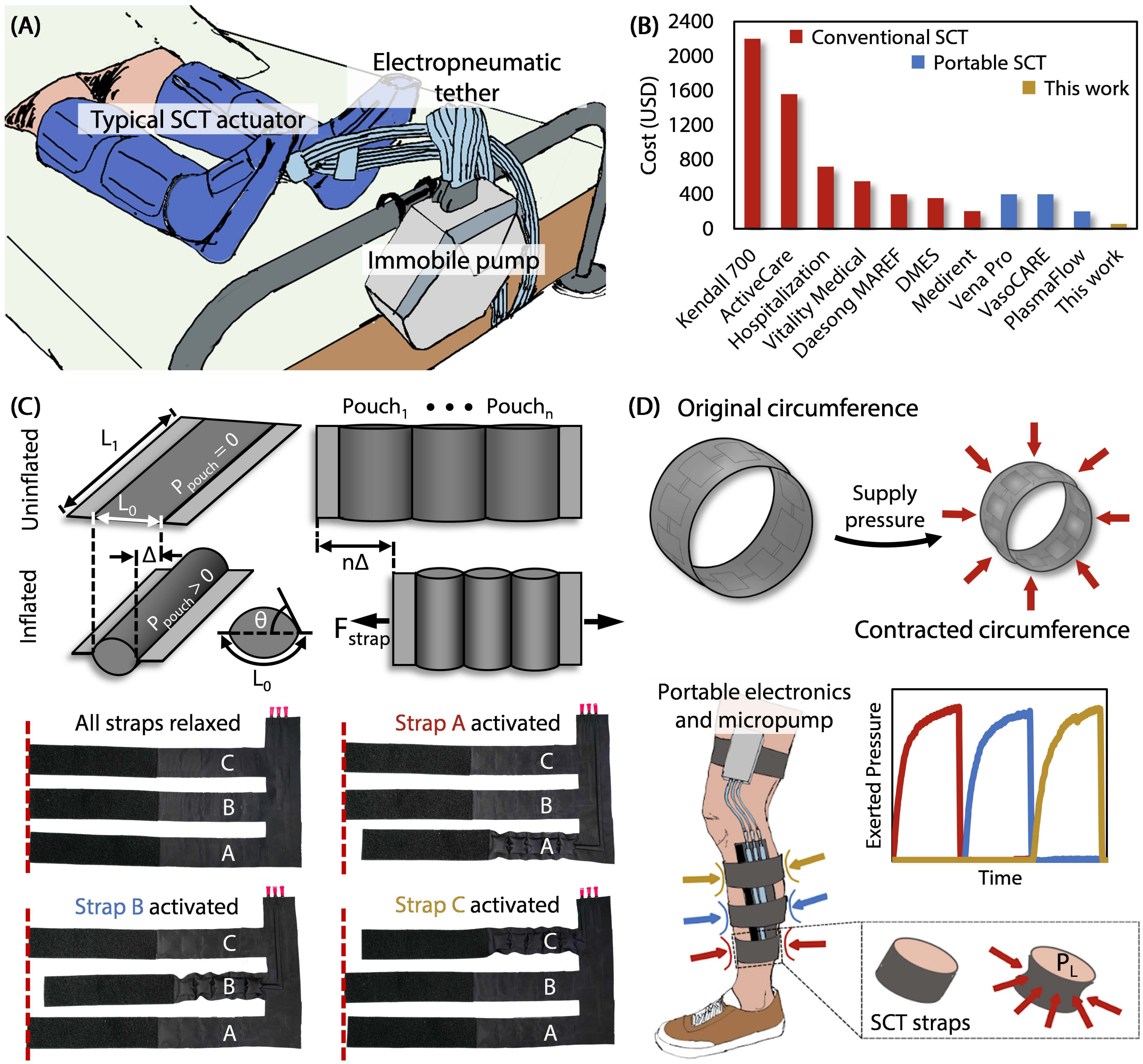

(A)
Electropneumatic tether
Typical SCT actuator
Immobile pump
(B)
Conventional SCT
Portable SCT
This work
Cost (USD)
2400
2000
1600
1200
800
400
0
Kendall 700
ActiveCare
Hospitalization
Vitality Medical
Daesong MAREF
DMES
Medirent
Vena Pro
VasoCARE
PlasmaFlow
This work
(C)
Uninflated
Inflated
Pouch1 • • • Pouchn
nΔ
Fstrap
All straps relaxed
Strap A activated
Strap B activated
Strap C activated
C
B
A
(D) Original circumference
Supply pressure
Contracted circumference
Portable electronics and micropump
Exerted Pressure
Time
SCT straps

Figure 2

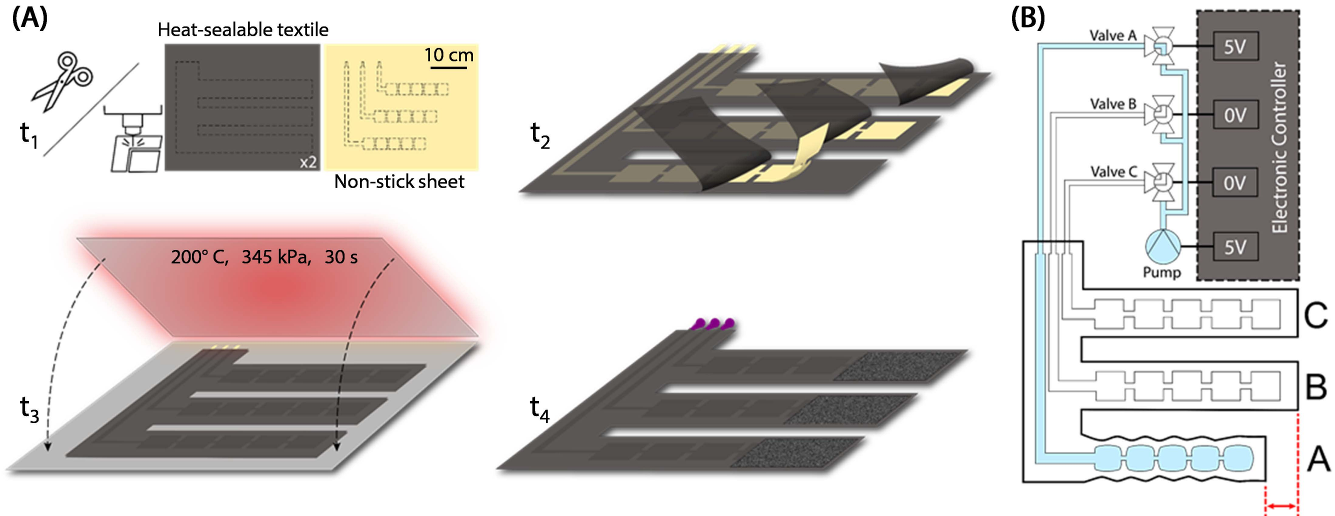

(A)
Heat-sealable textile
10 cm
x2
Non-stick sheet
t_1
t_2
200° C, 345 kPa, 30 s
t_3
t_4
(B)
Valve A
Valve B
Valve C
Pump
5V
0V
0V
5V
Electronic Controller
C
B
A

Figure 3

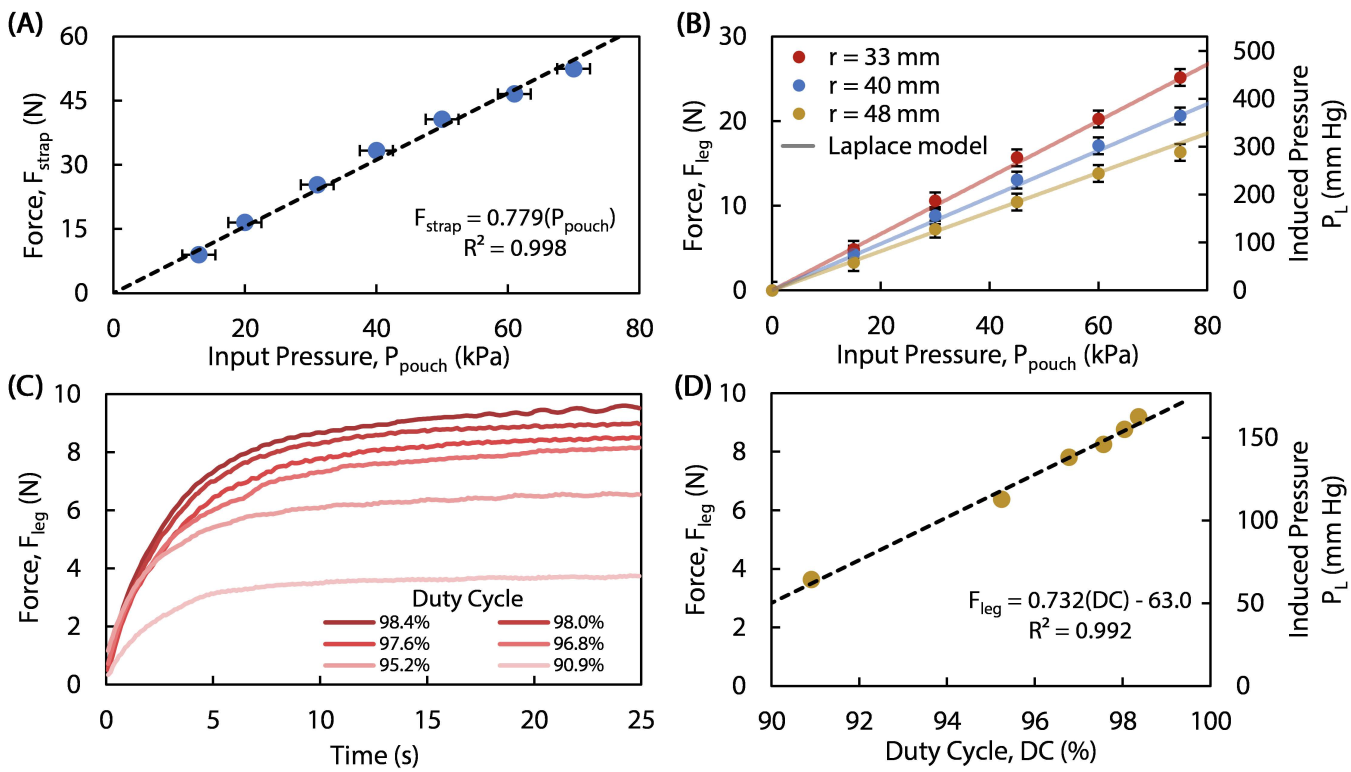

(A)
Force, F_{strap} (N)
Input Pressure, P_{pouch} (kPa)
$F_{strap} = 0.779(P_{pouch})$
$R^2 = 0.998$
(B)
r = 33 mm
r = 40 mm
r = 48 mm
Laplace model
Force, F_{leg} (N)
Input Pressure, P_{pouch} (kPa)
Induced Pressure P_L (mm Hg)
(C)
Force, F_{leg} (N)
Time (s)
Duty Cycle
98.4%
98.0%
97.6%
96.8%
95.2%
90.9%
(D)
Force, F_{leg} (N)
Duty Cycle, DC (%)
Induced Pressure P_L (mm Hg)
$F_{leg} = 0.732(DC) - 63.0$
$R^2 = 0.992$

Figure 4

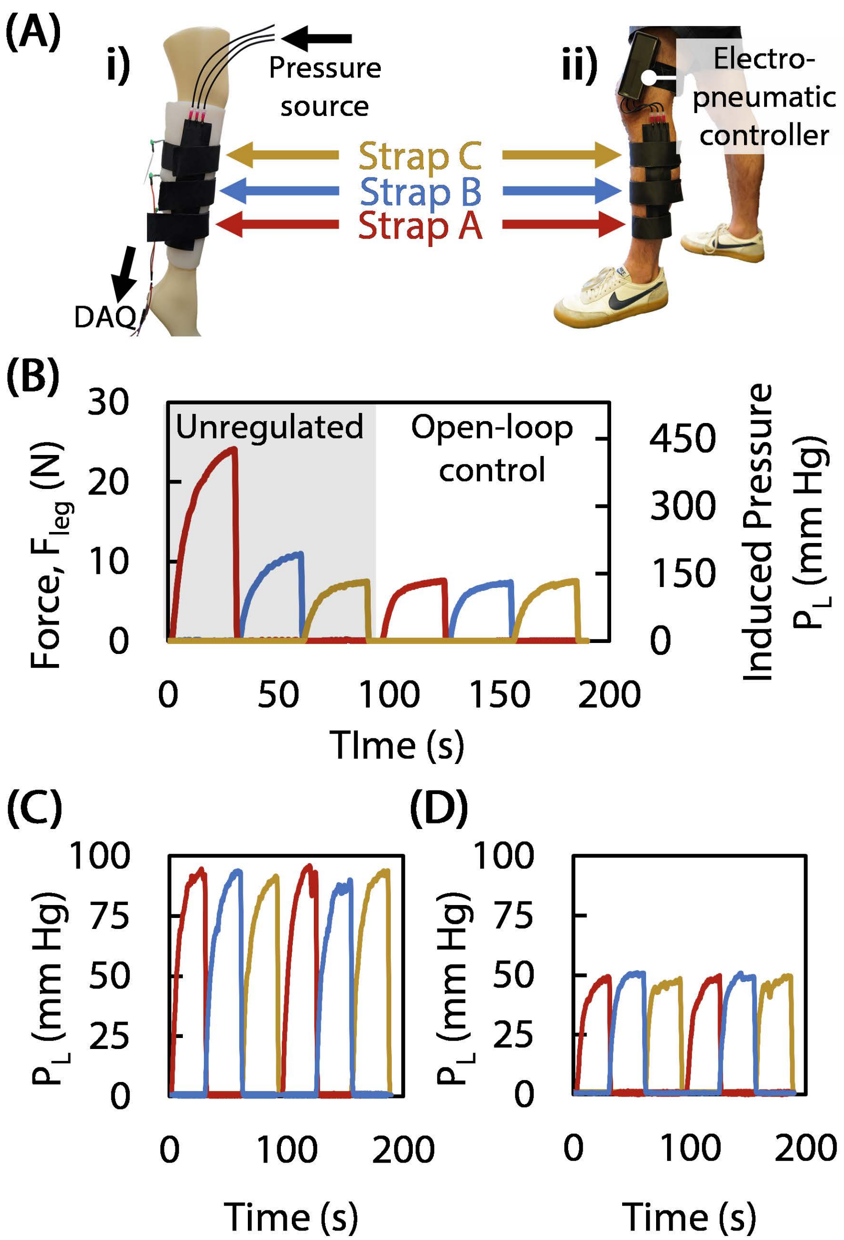
(A)
i)
Pressure source
DAQ
Strap C
Strap B
Strap A
ii)
Electro-pneumatic controller
(B)
Unregulated
Open-loop control
Force, F_{leg} (N)
30
20
10
0
450
300
150
0
Induced Pressure P_L (mm Hg)
0
50
100
150
200
TIme (s)
(C)
P_L (mm Hg)
100
75
50
25
0
0
100
200
Time (s)
(D)
P_L (mm Hg)
100
75
50
25
0
0
100
200
Time (s)

Supplementary Material

1 Supplementary Text

Experimental Procedures:

To measure the relationship between the lateral tensile force exerted by the pouch motors, F_{strap}, and the pneumatic input pressure, P_{pouch}, we used a universal testing machine (Instron, Model 68SC-2), an electronic pressure gauge (SSI Technologies, Model MGA-300-A-9V-R), and an in-house laboratory source of pressurized air. We secured the ends of the strap into the universal testing machine's grippers and set the testing method to prevent displacement (i.e., measuring blocked force), as shown in Figure S1. We connected the pneumatic inlet of the strap to the air supply, which was set to a specific pressure on a manual regulator, and we measured the lateral tensile force exerted by the strap via a 2 kN load cell integrated in the universal testing machine. We used the digital pressure gauge to measure the value of the supplied pneumatic pressure fed into the strap.

To experimentally determine the inward radial force exerted by the strap, F_{leg} (which is ultimately correlated directly to the Laplace pressure, P_L, applied to the leg), we used the following devices: a digital pressure gauge (SSI Technologies, Model MGA-300-A-9V-R), a data acquisition device (DAQ) (National Instruments, Model USB-6218), a force-sensing resistor (Interlink Electronics, FSR 402) with surface area of 1.77 cm^2, several solid cylinders of various diameters, a layer of silicone elastomer (Smooth-On, Dragon Skin 10 Very Fast), and a laboratory air supply. We adhered the force-sensing resistor to the outer face of one of the solid cylinders and then encompassed the cylinder by wrapping it with the sheet of elastomer to form a pseudo-appendage. Then, we wrapped one of the straps containing a pouch motor around the elastomer-wrapped cylinder and secured the strap using hook-and-loop fasteners. We pressurized the strap to a specific pressure by reading the digital pressure gauge. A surface area correction factor of α (in this work, valued at 2.4) was empirically determined when calculating the Laplace pressure from the input pressure to correct for distribution of force through the elastomer sheet onto the sensor. The DAQ, connected to both the sensor and a laptop, read the change in voltage of the sensing circuit and sent the corresponding data to the laptop. Using the manufacturer's provided technical documentation for the sensors, we calculated the exerted radial force based on the change in voltage in the circuit.

After finding the inward radial force on the solid cylinders, we ran a similar test on a mannequin leg to simulate and observe the device's operation on a geometry with better anatomical representation (main text Fig. 4a). The devices used were a DAQ (National Instruments, Model USB-6218), three force-sensing resistors (Interlink Electronics, FSR 402), a layer of silicone elastomer (Smooth-On, Dragon Skin 10 Very Fast), the electrical control system of the presented SCT device (main text Fig. 2b, Fig. S2), and a laptop running MATLAB. Similar to the test for the solid cylinders discussed above, we embedded the three force-sensing resistors underneath the elastomeric layer that was wrapped around the mannequin leg. After connecting the device to the electronic and pneumatic equipment, the device was used to apply sequential compression through the three straps. The DAQ sent the laptop the real-time data for the voltage for each of the force-sensing resistors and was then able to calculate the force exerted on the mannequin leg over time. We performed the same test with the device mounted on a human leg. Lastly, to understand the relationship between the exerted force and the duty cycle of the micropump (Skoocom, SC3101PM), we ran an experiment similar to the one described above investigating radial force on the mannequin leg in which we recorded the force for one strap. Different duty cycles (DC) were applied to the micropump, and the exerted force on the leg showed a linear relationship between exerted force and DC percentage (main text Fig. 3c, d), providing an empirically derived curve to relate these two quantities (main text Eq. 6 and Fig. 3d).

Details on the Fabrication Process:

The sheet-based portion of the device is constructed using the two scalable-vector-graphic (SVG) files provided: Intermediate_Layer.svg and Heat_Sealable_Layer.svg. Either file can be used as an input for a laser cutter or vinyl cutting device, which will cut the non-stick and TPU (or TPU-coated textile) layers of the device according to the geometry within the files. If neither device is available, the geometry can be drawn or printed on parchment paper and TPU-coated textile and then cut by hand using scissors. In this work, the widths and lengths of each pouch in the strap are $L_0 = L_1 = 3$ cm. Once the three layers are cut, they must be heat pressed together. Cardstock may be threaded through slotted alignment tabs on the layers to keep the layers aligned relative to each other during heat pressing. In this work, the layers were heat pressed for 30 seconds at 345 kPa and 200 ºC. If a heat press is not available, a standard clothes iron can be used. Once the device has cooled back to ambient temperature, three 16 ga x 1” blunt-tip dispensing needles with threaded (twist-to-connect) Luer lock tapers (CML Supply, 901-16-100) are inserted and glued into the three openings created by the non-stick channels in the common section of the heat-pressed stack. Next, hook-and-loop fasteners are attached to the end of the straps and to the common section, either with adhesive or stitching, such that when a strap wraps around the leg it can be secured tightly.

To fabricate the enclosure for the electrical components of the device, the provided files (Electrical_Box.STL, Electrical_Box_Top.STL) can be used to 3D print the box and its cover, respectively, out of polylactic acid (PLA) or other reasonably durable materials. After printing the box, a strip of fabric with hoop-and-loop fasteners can be threaded through the slit above the base of the box to act as a strap which mounts the box to the leg. Depending on the spatial management of the circuit components that are intended to fit inside the box, the casing may be altered before printing with free-to-download computer-aided design (CAD) programs.

To fabricate the emulated leg, we used a polyethylene mannequin leg (Econoco, 00841134106370) and a 1-cm-thick layer of silicone elastomer (Smooth-On, Dragon Skin 10 Very Fast). Following the provided instructions from Smooth-On, we mixed the elastomer components together and poured the resulting liquid into a rectangular plastic box, where it cured in its final 1-cm thickness. We calibrated three force-sensing resistors (Interlink Electronics, FSR 402) and embedded them between the elastomer and the mannequin’s leg. We used the provided MATLAB code (FSR_Record.m) to record the force data to a laptop connected to a DAQ (National Instruments, Model USB-6218). We ran the attached Arduino code (Leg_Force_Experiments.ino) onboard the Arduino Nano IOT 33 to supply the necessary pneumatic pressure, P_{pouch}, to the straps for our experiments.

Detailed model numbers for all the parts used are listed in Table S2 at the end of this document.

2 Supplementary Figures and Tables

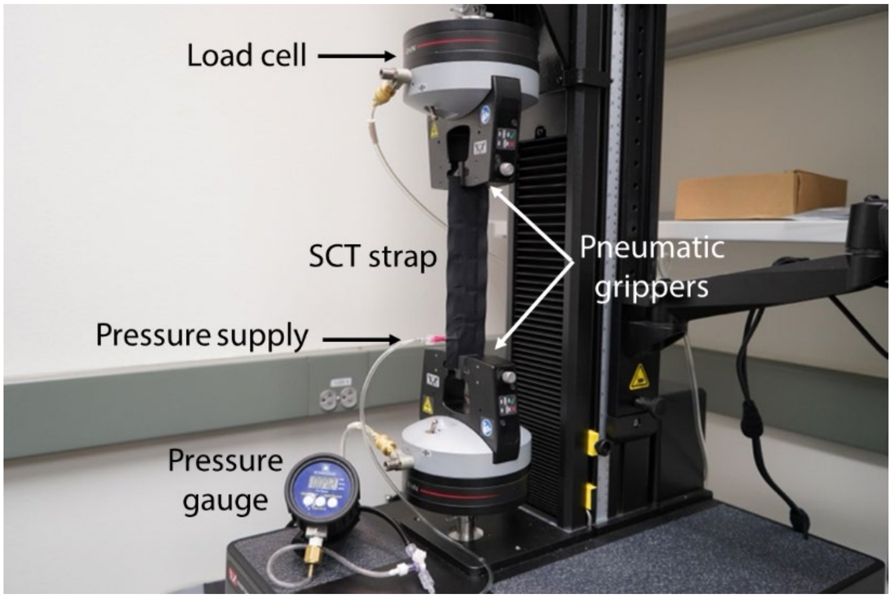

Figure S1. The setup for measuring the lateral (in-plane) force exerted by the pouch motor at a given pneumatic pressure input on a universal testing machine.

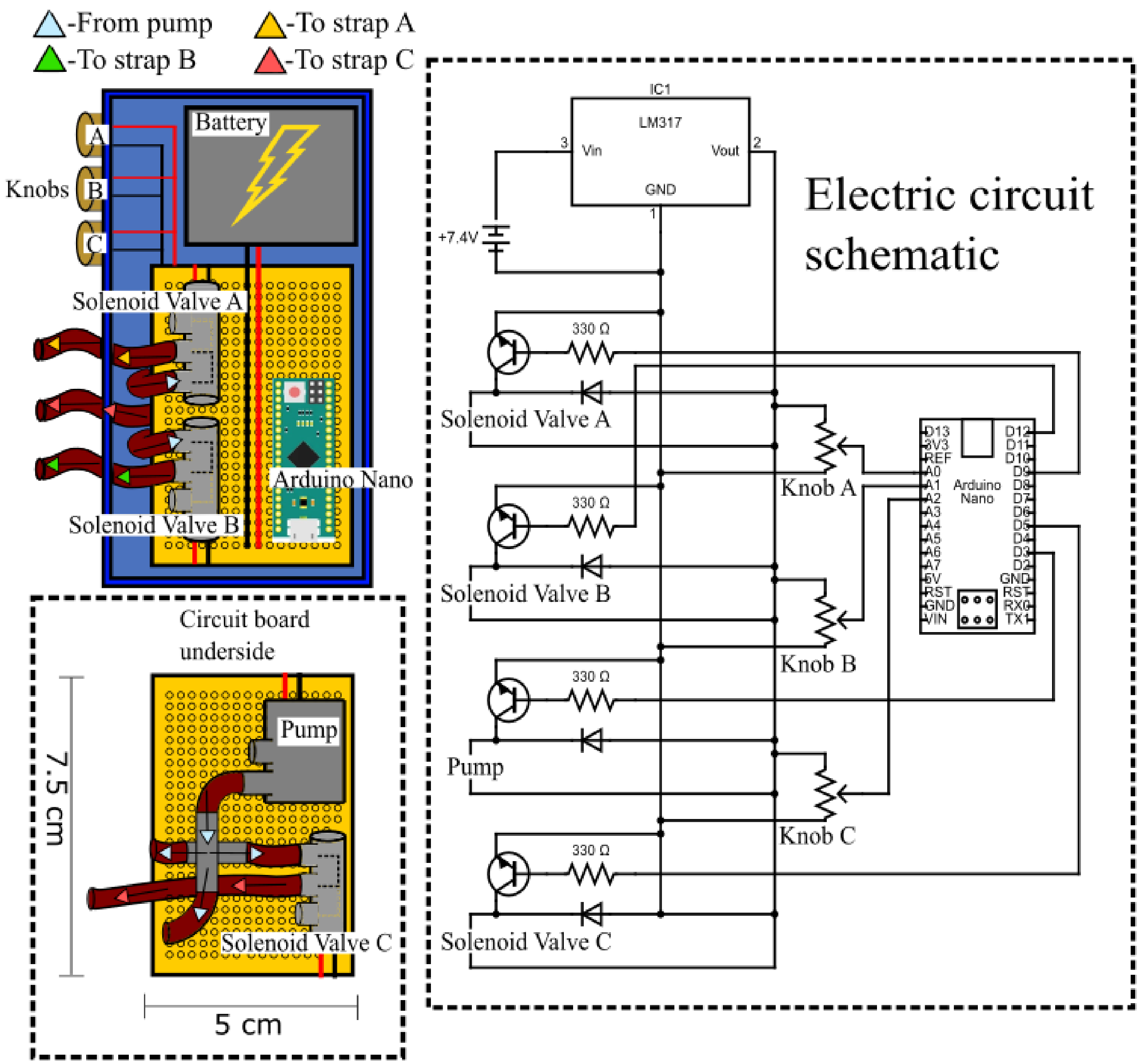

Figure S2. (Left) The thigh-mounted electropneumatic controller in Figure 4A(ii) contains a battery for electrical power, a pump for pneumatic power, solenoid valves for directing pressure to the straps, adjustable knobs to change the duty cycle of the pump (and the resulting applied pressure to the straps), and an Arduino Nano microcontroller to control all the inputs and outputs. (Right) The circuit diagram for the electronic wiring is shown.

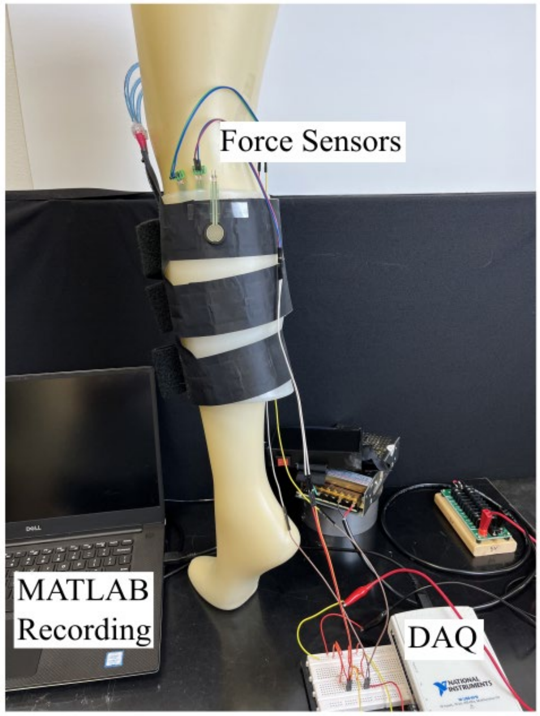

Figure S3. Experimental set up for bench testing Laplace pressures which shows the position of the force sensors. Two force sensors are recording and are embedded beneath both the elastomer and strap, while the third sensor has been placed on the outside of the uppermost strap to visualize the transverse position of the other two sensors beneath the elastomer.

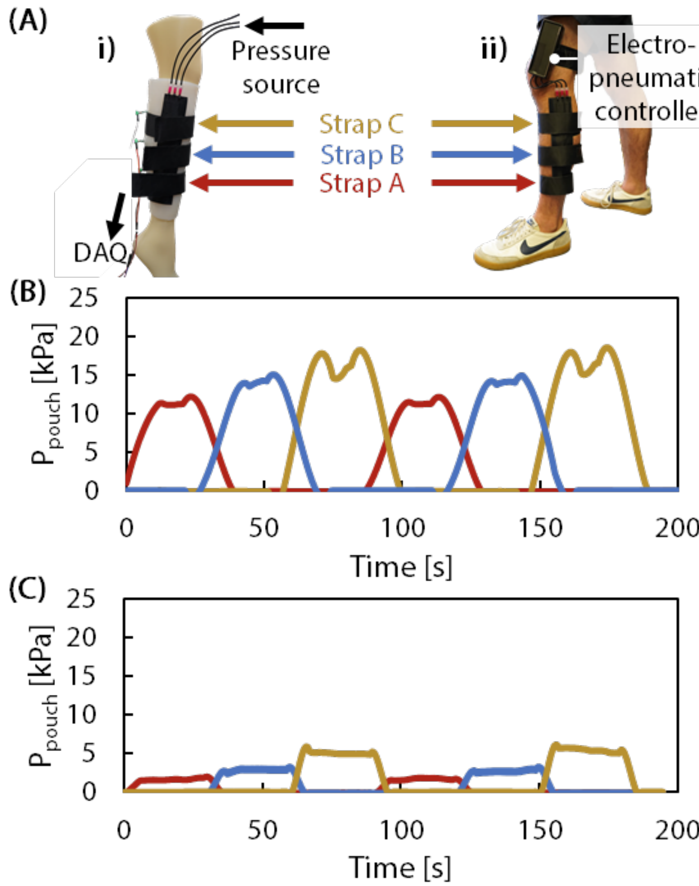

Figure S4. Input pressure (P_{pouch}) for each of the straps with open-loop control corresponding to the experimental results shown in Figure 4 in the main text. (**A-i**) The mannequin leg wears the SCT device, with a sensor measuring the F_{leg} between the leg and the Dragon Skin elastomer and pressure sensors (shown in Figure S4) measuring input pressure; (**A-ii**) a similar setup is attached to human leg with a thigh-mounted electropneumatic controller containing the micropump, solenoid valves, and microcontroller. (**B**) Open-loop controlled input pressure for the results seen in Figure 4C for the 90 mm Hg of P_{L}. (**C**) Open-loop controlled input pressure for the results seen in Figure 4D for the 50 mm Hg of P_{L}.

Table S2. The cost ($) of sequential compression therapy for different time frames. For the cost comparison provided in the manuscript, we selected 1 month as the time frame because it is a commonly suggested timespan for rehabilitation after surgery. However, some patients need long-term SCT, which would incur additional incremental costs for some of the choices such as hospitalization or equipment rentals. For those products that are widely available for rental, we used their rental prices, and therefore their costs are incremental in this chart. For other products, we used their one time purchase price. Note that Hospitalization column depicts the rental price of Kendall 700 plus medical service, as it is the dominant product used in the hospitals. The Kendall 700 column suggest the one-time purchase price of the Kendall 700. With longer timeframes, the low-cost benefit of the our SCT device becomes increasingly more advantageous.

Time Frame	Hospital -ization	DMES	Medirent	Kendall 700	Vitality Medical	Daesong-MAREF	Active -Care	Vena Pro	Plasma Flow	Vaso CARE	This work*
1 Week	260	190	98	2200	550	400	1560	400	200	400	56
1 Month	720	354	205	2200	550	400	1560	400	200	400	56
6 Months	3720	1426	905	2200	550	400	1560	400	200	400	56
1 Year	7420	2747	1745	2200	550	400	1560	400	200	400	56

Table S2. Major parts used in the presented device. Some minor parts, such as the exact model of PLA used in the printing of the electronic box, are not included in the table because those parts are easily replaceable by any similar products.

Part Names	**Model Number (#)**
Arduino Nano IOT 33	ABX00032
Skoocom Miniature Pneumatic Pump	SC3101PM
Lee Co. Pneumatic Valves	LHDA0531115H
Galaxy 2S (7.4V) 120 mAh Lipoly Battery Pack	UPC: 04429784075
Seattle Fabrics: Heat Sealable Coated Nylon Taffeta	FHST
Reynolds Kitchens Parchment Paper	G74991